Published in final edited form as:
J Cell Mol Med. 2014 November ; 18(11): 2165–2175. doi:10.1111/jcmm.12326.

Enhancement of Dynein-mediated Autophagosome Trafficking and Autophagy Maturation by ROS in Mouse Coronary Arterial Myocytes

Ming Xu[#], **Xiao-Xue Li**[#], **Yang Chen**, **Ashley L. Pitzer**, **Yang Zhang**, and **Pin-Lan Li**
Department of Pharmacology and Toxicology, School of Medicine, Virginia Commonwealth University, Richmond, VA, 23298

[#] These authors contributed equally to this work.

Abstract

Dynein-mediated autophagosome (AP) trafficking was recently demonstrated to contribute to the formation of autophagolysosomes (APLs) and autophagic flux process in coronary arterial myocytes (CAMs). However, it remains unknown how the function of dynein as a motor protein for AP trafficking is regulated under physiological and pathological conditions. The present study tested whether the dynein-mediated autophagy maturation is regulated by a redox signaling associated with lysosomal Ca^{2+} release machinery. In primary cultures of CAMs, reactive oxygen species (ROS) including H_2O_2 and $O_2^{-\cdot}$ (generated by xanthine/xanthine oxidase) significantly increased dynein ATPase activity and APs movement, which were accompanied by increased lysosomal fusion with APs and APL formation. Inhibition of dynein activity by (erythro-9-(2-hydroxy-3-nonyl)adenine) (EHNA) or disruption of the dynein complex by dynamitin (DCTN2) overexpression blocked ROS-induced dynein activation, APs movement and APLs formation, and resulted in an accumulation of APs along with a failed breakdown of APs. Antagonism of nicotinic acid adenine dinucleotide phosphate (NAADP)-mediated Ca^{2+} signaling with NED-19 and PPADS abolished ROS-enhanced lysosomal Ca^{2+} release and dynein activation in CAMs. In parallel, all these changes were also enhanced by overexpression of NADPH oxidase-1 (Nox1) gene in CAMs. Incubation with high glucose led to a marked $O_2^{-\cdot}$ production compared with normoglycemic CAMs, while Nox1 inhibitor ML117 abrogated this effect. Moreover, ML117 and NED-19 and PPADS significantly suppressed dynein activity and APL formation caused by high glucose. Taken together, these data suggest that ROS function as important players to regulate dynein-dependent APs trafficking leading to efficient autophagic maturation in CAMs.

Keywords

Dynein; Autophagy maturation; ROS; NAADP; coronary arterial myocyte; High glucose

Correspondence sent to: Pin-Lan Li, MD, PhD, Department of Pharmacology and Toxicology, Medical College of Virginia, Virginia Commonwealth University, 1220 East Broad Street, P.O. Box 980613, Richmond, VA 23298; Tel. 804 828-4793; Fax: 804 828-2117; pli@vcu.edu.

Conflict of interest None.

Introduction

Autophagy (also known as macroautophagy) is a cellular catabolic pathway leading to lysosomal degradation and recycling of proteins and organelles in eukaryotes [1]. A crucial step during autophagic flux is autophagy maturation, a process of autophagosomes (APs) trafficking and fusion with lysosomes to form autophagolysosomes (APLs)[2–4]. Autophagy-related (Atg) genes have been identified to play essential roles for the formation of autophagosomes (APs). However, the molecular mechanisms underlying autophagy maturation are relatively understudied. We recently demonstrated that dynein, a multi-subunit cytoplasmic motor protein, mediates APs trafficking which contributes to the formation of autophagolysosomes (APLs) under proatherogenic stimulation in coronary arterial myocytes (CAMs)[5]. However, it remains unknown how dynein's function as a motor protein for AP trafficking is regulated in these vascular cells and whether such role dynein is involved in autophagy maturation under other pathological conditions such as hyperglycemia.

Recently, reactive oxygen species (ROS) have been shown to interact with autophagy machinery [6]. Increased generation of ROS and cellular oxidative stress by various stimuli serves as important triggering mechanisms to induce autophagy [6–9]. One mechanism for enhanced oxidative stress to trigger autophagy is through modulating Atg4 activity by oxidizing a critical cysteine residue in this protein [10]. Atg4 cleaves LC3 to expose its C-terminal glycine to form conjugates with phosphatidylethanolamine by an ubiquitin-like system [11]. Thus, redox regulation of Atg4 activity modulates the incorporation process of lipidated LC3 proteins into the autophagosomal membrane and subsequent AP formation as shown under starvation conditions [10]. Reciprocally, ROS-activated autophagy pathway can protect cells from intensive oxidative stress by eliminating ROS-producing compartments such as dysfunctional mitochondria [12]. Thus, a complex interplay between ROS and autophagy pathways may exist under various pathological conditions such as nutrition deprivation and hyperglycemia. Despite ROS having been shown to regulate autophagy induction and APs formation at the early stage of autophagy, it remains elusive whether or how ROS modulate autophagy maturation, an event at the late stage of autophagy.

The present study tests the hypothesis that ROS may promote autophagy maturation via regulating dynein-mediated APs trafficking. Our data first demonstrated that ROS results in the activation of dynein ATPase. Then, we determined whether ROS-triggered APs trafficking and fusion with lysosomes is dependent on the activation of dynein ATPase, which is associated with NAADP-dependent lysosomal Ca^{2+} release. Lastly, we examined whether dynein-dependent APs trafficking is involved in autophagy maturation caused by high glucose-induced ROS production.

Materials and methods

Mice

Mice were purchased from the Jackson Laboratory. Eight-week old male and female mice were used in all experiments. All experimental protocols were reviewed and approved by the Institutional Animal Care and Use Committee of Virginia Commonwealth University.

Isolation and culture of mouse CAMs

CAMs were isolated from mice as previously described [13]. In brief, mice were deeply anesthetized with an intraperitoneal injection of pentobarbital sodium (25 mg/kg). The heart was excised with an intact aortic arch and immersed in a petri dish filled with ice-cold Krebs-Henseleit (*KH*) solution (in mM: 20 HEPES, 128 NaCl, 2.5 KCl, 2.7 $CaCl_2$, 1 $MgCl_2$, 16 glucose, pH 7.4). A 25-gauge needle filled with Hank's buffered saline solution (HBSS) (in mM: 5.0 KCl, 0.3 KH_2PO_4, 138 NaCl, 4.0 $NaHCO_3$, 0.3 $Na_2HPO_4 \cdot 7H_2O$, 5.6 D-glucose, and 10.0 HEPES, with 2% antibiotics) was inserted into the aortic lumen while the whole heart remained in the ice-cold buffer solution. The tip of the needle was inserted deep into the heart near the aortic valve. The needle was tied in place with the needle tip as close to the base of the heart as possible. The infusion pump was started with a 20-ml syringe containing warm HBSS through an intravenous extension set at a rate of 0.1 ml/minute for 15 minutes. HBSS was replaced with a warm enzyme solution (1 mg/ml collagenase type I, 0.5 mg/ml soybean trypsin inhibitor, 3% BSA, and 2% antibiotic-antimycotic), which was flushed through the heart at a rate of 0.1 ml/minute. Perfusion fluid was collected at 30-, 60-, and 90-minute intervals. At 90 minutes, the heart was cut with scissors and the apex was opened to flush out the cells that collected inside the ventricle. The fluid was centrifuged at 1, 000 rpm for 10 minutes, the cell-rich pellets were mixed with the one of the media described below, and the cells were plated on 2% gelatin-coated six-well plates and incubated in 5% CO_2-95% O_2 at 37°C. DMEM supplemented with 10% FBS, 10% mouse serum, and 2% antibiotics was used to culture isolated smooth muscle cells. The medium was replaced three days after cell isolation and then once or twice each week until the cells grew to confluence. As previously described [14], mouse CAMs were identified according to their morphology, immunohistological staining, Western blot analysis of marker proteins, and flow cytometric characteristics.

Nucleofection of DCTN2 cDNA and Nox1 cDNA

Both dynamitin (Dynactin 2: DCTN2) cDNA (Catalog# MC200162) and Nox1cDNA plasmids (Catalog# MG226022) were purchased from OriGene Technologies. DCTN2 cDNA plasmid contains a full-length DCTN2 gene (1653 bp) under a cytomegalovirus (CMV) promoter. Nox1cDNA plasmid contains a full-length Nox1 gene (1692 bp) under a CMV promoter. Transfection of plasmid was performed using a 4D Nucleofector X-Unit (Lonza, CA, USA) according to the manufacturer's instructions as we previously described [15]. Briefly, CAMs were tyrpsinized and centrifuged at 90×*g* for 10 minutes. The cell pellet was resuspended in 100 μL P1 Nucleofection solutions (Lonza) for Nucleofection (with the program code CM137). The program was chosen based on the fact that Nucleofection efficiency was over 80% as analyzed by flow cytometry using control GFP plasmids. For each Nucleofection sample, 2 μg plasmid DNA was added in 100 μL P1 Nucleofection

solution. After Nucleofection, the cells were cultured in DMEM medium for 24 hours and then were ready for treatment. The efficiency of DCTN2cDNA and Nox1cDNA transfection was assessed by Western blot analyses.

Assay of cytoplasmic dynein ATPase activity

Dynein in mouse CAMs was purified using a published protocol with slight modification [16]. Cytoplasmic protein of mouse CAMs was extracted with ice-cold extraction buffer (250 ml of 0.05 M PIPES-NaOH, 0.05 M HEPES, pH 7.0, containing 2 mM $MgC1_2$, 1 mM EDTA, 1 mM phenylmethylsulfonyl fluoride (PMSF), 10 μg/ml leupeptin, 10μg/ml tosyl arginine methyl ester (TAME), 1 μg/ml pepstatin A, and 1 mM dithiothreitol (DTT). Exogenous taxol (20 μM) was added to 20 mL of cell extract containing 4 mg/mL cytoplasmic protein, which was incubated in a 37°C water bath (with occasional swirling) for 12 minutes. The cell extract was underlayered with a prewarmed 7.5% sucrose solution, and then centrifuged at 60,000 *g* for 30 minutes at 35°C. The supernatant was removed and the pellet was resuspended in 10 mL of extraction buffer containing 3 mM MgGTP and 5 μM taxol to release kinesin and dynamin. The resuspended pellet was incubated for 15 minutes prior to centrifugation at 60,000 *g* for 30 minutes. The supernatant was removed, and the pellet was resuspended in 1.25 mL of extraction buffer containing 10 mM Mg-ATP for 10 minutes at 37°C. The resuspended pellet was centrifuged at 200,000 *g* for 30 minutes at 25°C. The supernatant containing ATP-released cytoplasmic dynein was used for sucrose density gradient fractionation. Cytoplasmic dynein may constitute up to 50% of total protein in the ATP extract, the remainder consisting of tubulin and a low level of fibrous microtubule-associated proteins (MAPs). 1 mL ATP extract was further centrifuged on 10 mL of a 5–20% sucrose gradient in fractionation buffer (20 mM Tris-HCl, pH 7.6, 50 mM KCl, 5 mM $MgSO_4$, 0.5 mM EDTA and 1 mM DTT) at 125,000 *g* for 16 h at 4°C. Eleven 1 mL fractions were collected from the bottom of the tube. The dynein fraction peak was at about fraction 5, well resolved from the other tubulin and MAPs.

The assays of dynein ATPase activity were performed in 50 μL reaction mixtures containing 20 mM Tris-HCl (pH 7.6), 50 mM KCl, 5 mM $MgSO_4$, 0.5 mM EDTA and 1 mM DTT [17]. In a standard assay condition, 10 μL of enzyme fractions and 4 mM of ATP were incubated with assay buffer at 37 °C for 40 minutes. The reaction was then stopped using highly acidic malachite green reagent, and the absorbance was read at 660 nm in spectrophotometer (Elx800, Bio-Tek). The amount of inorganic phosphate release in the enzymatic reaction was calculated using the standard calibration curve generated with inorganic phosphate. The control in this assay contained all ingredients of the reaction mixture but the reaction was stopped at 0 time.

Dynamic analysis of AP movement in CAMs

CAMs (2×10^4/ml) cultured in a 35 mm dish were incubated with 12 μl BacMam GFP-LC3B virus particles at 37°C for 16 h to express the LC3B-GFP gene. The confocal fluorescent microscopic recording was conducted with an Olympus Fluoview System. The fluorescent images for APs (LC3B-GFP) in the CAMs were continuously recorded at an excitation/emission (nm) of 485/520 using the XYT recording mode with a speed of 1 frame/10 seconds for 10 minutes. Vesicle tracking was performed in MAGEJ using the LSM reader

and Manual tracking plugins according to the published protocol [18]. Ten vesicles with GFP-LC3B were chosen at random for each cell. These vesicles were then tracked manually for as long as they were visible, while the program calculated velocities for each frame. All the results were further calculated and analyzed in Excel. The number of cells with different velocity of APs was calculated.

Western blot analysis

Western blot analysis was performed as we described previously [15]. In brief, proteins from the CAMs were extracted using sucrose buffer [20 mM HEPES, 1mM EDTA, 255 mM sucrose, cocktail o protease inhibitors (Roche), pH 7.4]. After boiling for 5 minutes at 95 °C in a 5× loading buffer, 30μg of total proteins were separated by a 12% sodium dodecyl sulfate-polyacrylamide gel electrophoresis (SDS-PAGE). The proteins of these samples were then electrophoretically transferred at 100 V for 1 hour onto a PVDF membrane (Bio-Rad, USA). The membrane was blocked with 5% nonfat milk in Tris-buffered saline-Tween 20. After washing, the membrane was probed with 1:1000 dilution of primary mouse or rabbit antibodies against DCTN2 (Santa Cruz), Nox1 (Santa Cruz), Lamp1 (Novus), or β-actin (Santa Cruz) overnight at 4 °C followed by incubation with horseradish peroxidase-labeled IgG (1:5000). The immuno-reactive bands were detected by chemiluminescence methods and visualized on Kodak Omat X-ray films. Densitometric analysis of the images obtained from X-ray films was performed using the Image J software (NIH).

Confocal microscopic analysis of co-localization of lysosomes with APs in live CAMs

To monitor the fusion of APs with lysosomes in live CAMs, APs and lysosomes were labeled with fluorescent proteins by introducing LC3B-GFP and Lamp1-RFP genes into CAMs. To this end, BacMam (baculovirus-based expression in mammalian cells) expression system was utilized to deliver and express LC3B-GFP and Lamp1-RFP genes in CAMs. Modified insect virus (baculovirus) expressing a fusion construct of LC3B-GFP (P36235, Invitrogen) or Lamp1-RFP (C10597, Invitrogen) were packaged as BacMam virus particle and purchased from Invitrogen. Briefly, CAMs (4×10^4/ml) cultured in 35 mm dish were incubated with 12 μl mixture of BacMam virus particles containing LC3B-GFP or Lamp1-RFP gene at 37°C for 24 hours. Then, the cells were replaced with fresh medium and ready for treatment. The fluorescent images for APs (LC3B-GFP) and lysosomes (Lamp1-RFP) in CAMs were recorded at an excitation/emission (nm) of 485/520 and 555/584. Then the co-localizations were visualized with confocal microscopy. The colocalization coefficient of LC3B-GFP and Lysosomes-RFP was analyzed with Image-Pro Plus 6.0 software as we previously described [19].

Flow cytometric detection of APs and APLs

The Cyto-ID Autophagy Detection Kit (Enzo Life Sciences) was used to detect APs[5]. Briefly, CAMs (1×10^5/ml) were collected and centrifuged (400 × *g*, 5 minutes) at the end of the treatment. Then, CAMs were incubated with 0.5 mL of freshly diluted Cyto-ID Green Detection Reagent (1:4000) for 30 minute at 37°C in the dark. Without washing, stained CAMs were run in the green (FL1) channel with a Guava Easycyte Mini Flow Cytometry System (Guava Technologies, Hayward, CA) and analyzed with Guava acquisition and

analysis software (Guava Technologies). The enhancement of Cyto-ID Green dye signal indicates an increase in APs.

In addition, acridine orange (Sigma) was used to detect APLs. CAMs (1×10^6/ml) were stained with acridine orange (1:5000) for 17 minutes. After washes, CAMs were harvested in phenol red-free growth medium. Green (510–530 nm) and red (>650 nm) fluorescence emission from 10^4 cells illuminated with blue (488 nm) excitation light was measured with Flow Cytometry System and analyzed with Guava acquisition and analysis software. The mean red/green fluorescence ratio was calculated to indicate the change of intracellular APLs.

Assays for lysosomal pH

To observe lysosomal alkalinization, we incubated CAMs in PBS buffer with or without 100 μM chloroquine for 30 minutes. The cells were then loaded with LysoSensor Green DND-189 (1 μM; Invitrogen) in PBS buffer for 15 minutes at 37°C. Cells were washed twice with PBS and immediately visualized with a confocal laser scanning microscope (Fluoview FV1000, Olympus, Japan).

Confocal Microscopic Analysis of co-localization of ubiquitin and p62 in CAMs

For confocal analysis, cultured CAMs were grown on glass coverslips, stimulated or unstimulated, fixed in 4% paraformaldehyde in phosphate-buffer saline (PFA/PBS) for 15 minutes. After being permeablized with 0.1% Triton X-100/PBS and rinsed with PBS, the cells were incubated overnight at 4 °C with indicated primary antibodies: mouse anti-ubiquitin and rabbit anti-p62 (1:200, Cell Signaling). After washing, the slides probed with primary antibodies and were then incubated with Alexa-488- or Alexa-555-labeled secondary antibodies for 1 hour at room temperature. The slides were mounted and subjected to examinations using sequential scanning on a laser scanning confocal microscope (Fluoview FV1000, Olympus, Japan), with photos being taken and the co-localization analyzed by the Image Pro Plus 6.0 software (Media Cybernetics, Bethesda, MD, USA). The summarized co-localization efficiency data was expressed as Pearson correlation coefficient (PCC) as described previously [19].

Fluorescent microscopic measurement of $[Ca^{2+}]_i$ in CAMs

A fluorescence image analysis system was used to determine intracellular Ca^{2+} concentration ($[Ca^{2+}]_i$) in CAMs with fura-2 acetoxymethyl ester (fura-2) as an indicator as previously described [14,20]. Having been loaded with 10 μM fura-2 at room temperature for 30 minutes, the cells were washed three times with Ca^{2+}-free Hank's buffer. The ratio of fura-2 emissions, when excited at the wavelengths of 340 and 380 nm, was recorded with a digital camera (Nikon Diaphoto TMD Inverted Microscope). Metafluor imaging and analysis software were used to acquire, digitize, and store the images for off-line processing and statistical analysis (Universal Imaging). The fluorescence ratio of excitation at 340 nm to that at 380 nm (F340/F380) was determined after background subtraction, and $[Ca^{2+}]_i$ was calculated by using the following equation: $[Ca^{2+}]_i = K_d\beta[(R - R_{min})/(R_{max} - R)]$, where K_d for the fura-2-Ca^{2+} complex is 224 nM; R is the fluorescence ratio (F_{340}/F_{380}); R_{max} and R_{min} are the maximal and minimal fluorescence ratios measured by addition of 10

μM of Ca^{2+} ionophore ionomycin to Ca^{2+}-replete solution (2.5 mM $CaCl_2$) and Ca^{2+} -free solution (5 mM EGTA), respectively; and β is the fluorescence ratio at 380-nm excitation determined at R_{min} and R_{max}, respectively. Lysosomal Ca^{2+} release was monitored indirectly by treating Fura-2-loaded CAMs with Glycyl-L-phenylalanine 2-naphthylamide (GPN, 200 μM), a tripeptide causing osmotic lysis of cathepsin C–positive lysosomes.

Confocal microscopic measurement of lysosome Ca^{2+} release

To detect lysosome Ca^{2+} release, sub-confluent CAMs in 35-mm cell culture dishes were incubated with dextran-conjugated tetramethylrhodamine (Rho; 1 mg/ml; Molecular Probes) for 4 h in DMEM medium containing 10% FBS at 37°C, 5% CO_2 followed by a 20-h chase in dye-free medium for lysosomes loaded with Rho, as previously described [21–22]. After being washed with Hank's buffered saline solution (HBSS) (in mM: 5.0 KCl, 0.3 KH_2PO_4, 138 NaCl, 4.0 $NaHCO_3$, 0.3 $Na_2HPO_4{\cdot}7H_2O$, 5.6 D-glucose, and 10.0 HEPES, with 2% antibiotics) three times, the Rho-loaded cells were then incubated with the Ca^{2+}-sensitive dye fluo-4 at a concentration of 5 μM. Ca^{2+} release and lysosome trace recordings were performed. Lysosome/Rho (Lyso/Rho) fluorescence images were acquired at 568-nm excitation and 590-nm emission. The co-localization coefficiency of Ca^{2+}/fluo-4 and Lyso/Rho was analyzed with Image-Pro Plus 6.0 software [23].

Statistics

Data are presented as means ± SE. Significant differences between and within multiple groups were examined using ANOVA for repeated measures, followed by Duncan's multiple-range test. The Students *t* test was used to detect significant differences between two groups. $P<0.05$ was considered statistically significant.

Results

ROS enhances dynein ATPase activity in CAMs

Dynein is a motor protein responsible for nearly all minus-end microtubule-based transport of vesicles in eukaryotic cells and has recently been implicated in APs trafficking and fusion with lysosomes to form APLs [5]. Superoxide ($O_2^{-\cdot}$) and hydrogen peroxide (H_2O_2) are the major ROS implicated in regulating autophagy [6]. Here, we demonstrated that treatment of CAMs with xanthine/xanthine oxidase (X/XO), a typical $O_2^{-\cdot}$ production system, or H_2O_2 resulted in a marked increase in dynein ATPase activity, which was significantly attenuated by EHNA, a dynein activity inhibitor (Figure 1A).

NADPH oxidase-generated ROS contribute to autophagy induction [24–26]. To examine whether endogenous ROS produced by NADPH oxidase has a similar effect to exogenous ROS on dynein activity, CAMs were transfected with NADPH oxidase isoform 1 (Nox1) cDNA plasmids. Nox1 cDNA transfection increased protein expression of Nox1 by 2.85-fold (Figure 1B). Consistently, $O_2^{-\cdot}$ production in CAMs was significantly increased after the Nox1 cDNA transfection, which was inhibited by NADPH oxidase inhibitor, diphenylen iodonium (DPI) (Figure 1C). Similar with exogenous ROS, overexpression of Nox1 increased production as well as dynein ATPase activity in CAMs (Figure 1D). However, both exogenous and Nox1-derived ROS had no effect on the protein expression of dynein.

Moreover, there was no significant change of dynein expression after the pretreatment with EHNA, which showed that inhibition of dynein function has no effects on the expressions of dynein (Figure 1E and Figure 1F).

Dynamic analysis to APs movement upon ROS stimulation

Next, we examined whether APs trafficking is a consequence of ROS-sensitive dynein activity. APs are formed randomly throughout the cytoplasm and then transported to the perinuclear region where they fuse with lysosomes[18]. Microtubule-associated protein 1 light chain 3 beta (LC3B) is a marker protein of APs, which is recruited to autophagosomal membranes during the formation of APs. We labeled APs in living CAMs with LC3B-GFP and monitored their movements upon ROS treatment. Typically, fluorescent images of CAMs were taken every 10 seconds (Figure 2A). Under control condition, APs moved bidirectionally, i.e. towards and away from the nucleus. When CAMs were treated with X/XO, the movement of APs was significantly enhanced (Figure 2B). The velocity of AP movement significantly increased from 0.03 mm/second to 0.08 mm/second. Similar effects were also found in H_2O_2 treated CAMs (data not shown). These ROS-induced APs movement (velocity-range between 0.04 mm/second and 0.07 mm/second) was completely inhibited in CAMs with DCTN2 overexpression, which causes disruption of the dynein complex. Similarly, endogenous ROS production by Nox1 overexpression increased the velocity of APs movement, which was inhibited by dynein inhibitor EHNA (Figure 2C).

Dynein contributes to ROS-induced APs fusion to lysosome

To directly observe the role of ROS-sensitive dynein activity on the fusion of APs with lysosomes in living cells, both LC3B-GFP and Lamp1-RFP (Lamp-1 is a lysosome marker protein) genes were introduced into CAMs to visualize APs (green puncta) and lysosomes (red puncta). Fusion of APs with lysosomes increases the colocalization of LC3B-GFP with Lamp1-RFP and yields yellow puncta. As shown in Figure 3A and Figure 3B, under control conditions, only a few yellow puncta were detected. Both X/XO and H_2O_2 treatment markedly increased the number of yellow puncta and the colocalization coefficient between LC3B-GFP and Lamp1-RFP indicating a higher fusion rate of lysosomes with APs. However, such ROS-induced AP-lysosome fusion was inhibited by DCTN2 overexpression. Similarly, Nox1 cDNA transfection markedly enhanced the AP-lysosome fusion, which was inhibited by dynein inhibitor EHNA (Figure 3C).

Dynein is involved in the ROS-induced APLs formation

The formation of APLs was also quantified using flow cytometry with a lysomotrophic dye, acridine orange, which accumulates in lysosomes with bright red fluorescence and shows bright green and dim red fluorescence in the cytoplasm and nucleolus. Since APLs accumulate more acridine orange than lysosomes, the red/green fluorescence ratio indirectly measures the change of intracellular APLs [27]. Figure 4A shows that CAMs treated with X/XO or H_2O_2 shifted up to the area with high red fluorescence intensity. Quantification of the data in Figure 4B indicated that X/XO or H_2O_2 significantly increased the red/green fluorescence ratio suggesting that APLs formation were increased, and these effects were abrogated by DCTN2 overexpression. Similarly, inhibition of dynein activity by EHNA markedly attenuated APLs formation induced by Nox1 overexpression (Figure 4C).

Consistently, ROS-induced APLs formation was inhibited by spautin-1, a potent small molecule inhibitor of APs formation (Figure 4D). In contrast, ROS-induced APLs formation was further enhanced by leupeptin, a lysosomal protease inhibitor that blocks APLs degradation without changing lysosomal pH (Figure 4D). This result indicates that ROS indeed increase the formation of APLs rather than inhibit their degradation. Increased AP-lysosome fusion by ROS may be associated with enhanced lysosome biogenesis or acidification. However, ROS had no effects on Lamp1 expression (Figure 4E) or lysosomal pH (Figure 4F), ruling out these possibilities. Moreover, DCTN2 overexpression had no effects on the expression of Lamp-1, which showed that inhibition of dynein function has no effects on the expressions of Lamp-1.

Dynein regulated APs accumulation and autophagic degradation upon ROS stimulation

The role of dynein on ROS-induced autophagy maturation was further investigated by evaluating the effects of dynein inhibition on APs accumulation and autophagic degradation. A Cyto-ID Green dye was used to selectively label APs, and the percentage of Cyto-ID-positive cells that correlates with the number of APs was analyzed by flow cytometry [28]. Figure 5A showed that X/XO or H_2O_2 increased the percentage of Cyto-ID-positive cells indicating that more APs were formed. Such increases were further augmented by dynein inhibitor EHNA suggesting that the loss of dynein function results in APs accumulation under ROS stimulation. Inclusion of granular ubiquitin or selective autophagy substrate p62 in APs of cells can be used to detect the breakdown of autophagic vesicles [29]. As shown in Figure 5C, compared to scramble transfected cells, CAMs transfected with DCTN2 cDNA exhibited much more yellow puncta and increased colocalization between ubiquitin and p62 upon X/XO or H_2O_2 treatment. This suggests a failed breakdown of APs in the absence of dynein activity. Similar results were found in CAMs transfected with Nox1 cDNA when dynein was inhibited by EHNA (Figure 5B and 5D).

ROS induced NAADP-sensitive Ca^{2+} release

NAADP-sensitive lysosomal Ca^{2+} release has been implicated in the regulation of dynein activity under proatherogenic stimulation[5]. To test whether lysosomal Ca^{2+} was involved in ROS-induced APs trafficking, fluorescent imaging analysis was used to measure the lysosomal Ca^{2+} release in CAMs. GPN was used to release Ca^{2+} from lysosomes by inducing their selective osmotic swelling. Both X/XO and H_2O_2 significantly increased GPN-induced Ca^{2+} release, which was blocked by NAADP antagonists NED-19 and PPADS (Figure 6A,B). Similar results were also found in CAMs transfected with Nox1cDNA (Figure 6C).

In addition, we measured the localization of Ca^{2+} around lysosomes by confocal microscopy after labeling cells with fluo-4 and rhodamine-red (Lyso/Rho) lysosomal marker. Ca^{2+} release regions co-localized with lysosomes as indicated by yellow spots formed by the close proximity of green fluo-4 signals and rhodamine-red (Figure 7A). Both X/XO and H_2O_2 significantly increased the colocalization coefficient of fluo-4-Ca^{2+} and Lyso/Rho, indicating an enhanced lysosomal Ca^{2+} release, while NAADP antagonist PPADS or NED-19 abolished these effects (Figure 7B). Similarly, enhanced lysosomal Ca^{2+} release in CAMs by Nox1 overexpression was blocked by NAADP antagonists (Figure 7C).

Lysosomal Ca^{2+} release regulates dynein ATPase activity in CAMs upon ROS stimulation

To determine how ROS regulate dynein ATPase activity, we first examined whether ROS can directly oxidize dynein to enhance its activity. To this end, the extracted cytoplasmic protein lysates from CAMs were incubated with X/XO and H_2O_2. Surprisingly, X/XO and H_2O_2 had no direct effects on dynein ATPase activity (Figure 8A). We then examined whether NAADP-mediated lysosomal Ca^{2+} signaling is an upstream event of ROS-enhanced dynein activation. Indeed, ROS-enhanced dynein ATPase activation was significantly attenuated when the intact CAMs were treated with NAADP antagonists NED-19 and PPADS (Figure 8B and 8C).

Nox1-regulated dynein activity mediates APLs formation under high glucose

Finally, we examined whether ROS-sensitive dynein ATPase controls autophagy maturation under high glucose conditions. High glucose treatment induces ROS production in vascular smooth muscle cells via activation of Nox1 [30]. Consistently, treatment of CAMs with high glucose (30 mM) resulted in a marked increase of $O_2^{-\cdot}$ that was inhibited by ML117, a Nox1 specific inhibitor (Figure 9A). Moreover, high glucose treatment significantly increased dynein ATPase activity in CAMs, which was significantly attenuated by ML117 or NAADP antagonist, NED-19 or PPADS (Figure 9B). Importantly, the increased APLs formation, as shown by increased red/green fluorescence ratio of acridine orange staining under high glucose treatment, was abolished by pretreatment of CAMs with Nox1 inhibitor ML117, NAADP antagonist NED-19 or PPADS, or dynein inhibitor EHNA (Figure 9C).

Discussion

The present study demonstrates that in CAMs, ROS enhance the activity of dynein ATPase, a microtubule motor protein, which promotes APs trafficking and fusion with lysosomes to form APLs contributing to autophagy maturation. NAADP-dependent lysosomal Ca^{2+} release plays a critical role in controlling dynein-mediated autophagy maturation under either redox or high glucose condition.

ROS are rapidly produced, short-lived, and diffusible reactive molecules and are traditionally considered as cellular damage factors. However, accumulating evidence suggests that under physiological conditions or in the early stage of oxidative damage, ROS also act as signaling molecules to mediate cellular responses such as autophagy by inducing APs formation [31]. Such role of ROS in autophagy is attributed to their interactions with Atg proteins such as oxidative regulation of Atg4, a crucial factor mediating LC3 lipidation [9]. However, the molecular mechanisms underlying the ROS-triggered maturation of APs to APLs are relatively unknown. Here, we demonstrated that treatment of mouse CAMs with ROS or overexpressing Nox1, a ROS-producing NADPH oxidase isoform, in these cells dramatically enhanced the dynein ATPase activity indicating that dynein could be a potential target protein for ROS to modulate autophagy maturation.

During autophagy maturation, *de novo* generated APs sequester cytoplasmic proteins and organelles, which are delivered to lysosomes for degradation[32]. In this process, APs show a rapid vectorial movement to the direction of the centrosome, where lysosomes are usually

concentrated [18]. Dynein is a microtubule associated motor protein involved in AP trafficking in mammalian cells [2,5,18,33–34]. Inhibition or loss of dynein function impairs AP trafficking in glioma or neuronal cells [35]. The present study demonstrated that both exogenous and Nox1-derived ROS increased the movement of APs in CAMs, which was inhibited by either dynein inhibitor EHNA or disruption of the dynein complex with dynamitin (gene symbol is DCTN2) overexpression. These data suggest that dynein-mediated AP trafficking is also regulated by ROS. Since APs trafficking promotes APs fusion with lysosomes, we further observed increased colocalization of APs with lysosomes induced by ROS using LC3B-GFP and Lamp1-RFP transfected CAMs (Figure 3). In addition, increased fusion of LC3B-GFP with Lamp1-RFP by ROS was confirmed by showing increased APLs formation by ROS using acridine orange staining (Figure 4A–D). As a consequence of impaired AP trafficking, both ROS-induced AP-lysosome fusion and APLs formation were blocked by inhibition of dynein or disruption of dynein complex. Thus, our data suggest that redox regulation of the dynein activity controls autophagy maturation through APs trafficking and fusion with lysosomes.

Autophagy maturation results in the formation of functional APLs that break down their autophagic contents and ultimately themselves by lysosomal proteases. Inhibition of dynein function increased APs accumulation in glioma and neuronal cells [35], which indicates that accumulated APs due to an impaired autophagic degradation pathway is a characteristic of insufficient autophagy maturation. In the present study, we directly monitored the number of APs by flow cytometry using Cyto-ID Green probes and found that ROS-induced APs formation was further augmented by either EHNA or dynamitin overexpression indicating more APs were accumulated by ROS in the absence of dynein function. During autophagy, the p62 protein, an ubiquitin-binding scaffold protein, targets ubiquitinated protein aggregates to APs for autophagic degradation [29]. Thus, we also detected the breakdown of autophagic vesicles by determining the inclusion of granular ubiquitin or p62 in APs [36]. Our data revealed that ROS treatment resulted in more ubiquitin and p62 in APs with dynein inhibition suggesting that a failed breakdown of autophagic vesicles leads to APs accumulation. Together, these results further support the view that dynein-mediated APs trafficking and fusion with lysosomes contributes to ROS-induced autophagy maturation leading to an efficient autophagic degradation pathway.

Another important finding of the present study is the critical role of lysosomal Ca^{2+} release machinery in mediating ROS-induced dynein activation. In present study, we first demonstrated that ROS did not regulate dynein ATPase activity via direct oxidization of its subunits or interacting proteins in a cell-free system (extracted cytoplasmic proteins from CAMs were treated with ROS) (Figure 8A). Previous studies have reported that direct binding of Ca^{2+} to dynein complex regulates dynein motor function and the distribution of cytoplasmic dynein [37–38]. NAADP, a CD38-ADP-ribosylcyclase product, is one of the most potent intracellular Ca^{2+} mobilizing molecules, which regulates lysosomal Ca^{2+} release and lysosome function [39–41]. Previous study had demonstrated that exogenous $O_2^{-\cdot}$ increase ADP-ribosylcyclase activity, cADPR production, leading to mobilization of intracellular Ca^{2+} from the SR in mouse CAMs [42]. Recently, it was demonstrated that endogenous Nox1-derived $O_2^{-\cdot}$ serves in an autocrine fashion to enhance CD38 internalization, leading to redox activation of CD38/ADP-ribosylcyclase activity and

NAADP production [40]. Thus, these previous studies suggest ROS-induced NAADP signaling is initiated via redox activation of CD38/ADP-ribosylcyclase. In the present study, NAADP antagonists NED-19 or PPADS markedly reduced ROS-induced augmentation of lysosomal Ca^{2+} release and dynein activity in CAMs. Therefore, our data suggest that ROS function as signaling molecules to regulate dynein activity via enhancing NAADP-mediated lysosomal Ca^{2+} release.

The present study further revealed a critical role of dynein-mediated APs trafficking machinery in autophagy maturation associated with oxidative stress under pathological conditions such as high glucose. Hyperglycemia is a major causative factor in the development of diabetes-associated diseases. NADPH oxidase-associated oxidative stress has been identified as an important mechanism in the pathogenesis of hyperglycemia-induced vascular damage [43]. Previous studies revealed that Nox1 is a major NADPH oxidase isoform responsible for high glucose-induced $O_2^{-\cdot}$ production in vascular smooth muscle cells [30]. We consistently demonstrated that specific Nox1 inhibitor ML117 abolished high glucose-induced $O_2^{-\cdot}$ production, dynein activation, and APLs formation. In addition, NAADP antagonists and dynein inhibitor mimicked the effects of ML117 on APLs formation, therefore, our data suggest that Nox1-dervied ROS/NAADP-Ca^{2+}/dynein axis is involved autophagy maturation under high glucose condition in CAMs. Recent studies have suggested that moderately enhanced autophagy in vascular smooth muscle cells during early developmental stage of atherosclerosis may have beneficial effects by maintaining these cells into a more differentiated and contractile phenotype, thereby decreasing cell proliferation and preventing fibrosis[15]. In this respect, the signaling role of mild ROS production in promoting dynein-mediated autophagy maturation in CAMs may be protective at the early developmental stage of coronary atherosclerosis secondary to diabetes mellitus. Conversely, excessive ROS production may directly cause lysosomes damage leading to defective autophagy, which results in accumulation of dysfunctional organelles, such as mitochondria, exaggerating the oxidative damages in the vasculature [44–45]. Our study may also provide novel insights into understanding the role of autophagy in diabetes. It has been demonstrated that enhanced autophagy compensates the excessive insulin production in β-cells via accelerating autophagic degradation of insulin-containing β-granules [46]. Therefore, ROS promoted autophagy maturation may contribute to the maintenance of intracellular insulin content in β-cells in the settings of insulin secretory dysfunction, such as type 2 diabetes.

In conclusion, we demonstrated that in CAMs NAADP-lysosomal Ca^{2+}-regulated dynein activity plays an essential role in ROS-induced autophagy maturation by controlling the trafficking of APs and lysosomes to encounter each other leading to APLs fusion and formation. In addition, ROS/NAADP-Ca^{2+}/dynein signaling cascade also contributes to autophagy maturation under high glucose condition implicating a protective role of ROS-sensitive dynein activity during the early stages of hyperglycemia.

Acknowledgments

The study was supported by grants from the National Institute of Health (HL057244, HL075316, HL091464 and HL122937).

References

1. Levine B, Kroemer G. Autophagy in the pathogenesis of disease. Cell. 2008; 132:27–42. [PubMed: 18191218]
2. Xie Z, Klionsky DJ. Autophagosome formation: core machinery and adaptations. Nat Cell Biol. 2007; 9:1102–9. [PubMed: 17909521]
3. Melendez A, Neufeld TP. The cell biology of autophagy in metazoans: a developing story. Development. 2008; 135:2347–60. [PubMed: 18567846]
4. Reggiori F, Klionsky DJ. Autophagy in the eukaryotic cell. Eukaryot Cell. Feb; 2002 1(1):11–21. [PubMed: 12455967]
5. Xu M, Li XX, Xiong J, et al. Regulation of Autophagic Flux by Dynein-mediated Autophagosomes Trafficking in Mouse Coronary Arterial Myocytes. Biochim Biophys Acta. 2013; 1833:3228–36. [PubMed: 24095928]
6. Essick EE, Sam F. Oxidative stress and autophagy in cardiac disease, neurological disorders, aging and cancer. Oxid Med Cell Longev. 2010; 3:168–77. [PubMed: 20716941]
7. Yuan H, Perry CN, Huang C, et al. LPS-induced autophagy is mediated by oxidative signaling in cardiomyocytes and is associated with cytoprotection. Am J Physiol Heart Circ Physiol. 2009; 296:H470–9. [PubMed: 19098111]
8. Ye YC, Wang HJ, Yu L, et al. RIP1-mediated mitochondrial dysfunction and ROS production contributed to tumor necrosis factor alpha-induced L929 cell necroptosis and autophagy. Int Immunopharmacol. 2012; 14:674–82. [PubMed: 23000518]
9. He C, Zhu H, Zhang W, et al. 7-Ketocholesterol induces autophagy in vascular smooth muscle cells through Nox4 and Atg4B. Am J Pathol. 2013; 183:626–37. [PubMed: 23770348]
10. Scherz-Shouval R, Shvets E, Fass E, et al. Reactive oxygen species are essential for autophagy and specifically regulate the activity of Atg4. EMBO J. 2007; 26:1749–60. [PubMed: 17347651]
11. Ichimura Y, Kirisako T, Takao T, et al. A ubiquitin-like system mediates protein lipidation. Nature. 2000; 408:488–92. [PubMed: 11100732]
12. Moreau K, Luo S, Rubinsztein DC. Cytoprotective roles for autophagy. Curr Opin Cell Biol. 2010; 22:206–11. [PubMed: 20045304]
13. Teng B, Ansari HR, Oldenburg PJ, et al. Isolation and characterization of coronary endothelial and smooth muscle cells from A1 adenosine receptor-knockout mice. Am J Physiol Heart Circ Physiol. 2006; 290:H1713–20. [PubMed: 16299260]
14. Xu M, Zhang Y, Xia M, et al. NAD(P)H oxidase-dependent intracellular and extracellular O2*- production in coronary arterial myocytes from CD38 knockout mice. Free Radic Biol Med. 2012; 52:357–65. [PubMed: 22100343]
15. Wei YM, Li X, Xu M, et al. Enhancement of autophagy by simvastatin through inhibition of Rac1-mTOR signaling pathway in coronary arterial myocytes. Cell Physiol Biochem. 2013; 31:925–37. [PubMed: 23817226]
16. Paschal BM, Shpetner HS, Vallee RB. Purification of brain cytoplasmic dynein and characterization of its in vitro properties. Methods Enzymol. 1991; 196:181–91. [PubMed: 1827862]
17. Kumar S, Lee IH, Plamann M. Two approaches to isolate cytoplasmic dynein ATPase from Neurospora crassa. Biochimie. 2000; 82:229–36. [PubMed: 10863006]
18. Jahreiss L, Menzies FM, Rubinsztein DC. The itinerary of autophagosomes: from peripheral formation to kiss-and-run fusion with lysosomes. Traffic. 2008; 9:574–87. [PubMed: 18182013]
19. Xia M, Zhang C, Boini KM, et al. Membrane raft-lysosome redox signalling platforms in coronary endothelial dysfunction induced by adipokine visfatin. Cardiovasc Res. 2011; 89:401–9. [PubMed: 20823276]
20. Zhang F, Zhang G, Zhang AY, et al. Production of NAADP and its role in Ca2+ mobilization associated with lysosomes in coronary arterial myocytes. Am J Physiol Heart Circ Physiol. 2006; 291:H274–82. [PubMed: 16473958]
21. Bright NA, Gratian MJ, Luzio JP. Endocytic delivery to lysosomes mediated by concurrent fusion and kissing events in living cells. Curr Biol. 2005; 15:360–5. [PubMed: 15723798]

22. Zhang F, Xia M, Li PL. Lysosome-dependent Ca(2+) release response to Fas activation in coronary arterial myocytes through NAADP: evidence from CD38 gene knockouts. Am J Physiol Cell Physiol. 2010; 298:C1209–16. [PubMed: 20200208]
23. Zinchuk V, Zinchuk O, Okada T. Quantitative colocalization analysis of multicolor confocal immunofluorescence microscopy images: pushing pixels to explore biological phenomena. Acta Histochem Cytochem. 2007; 40:101–11. [PubMed: 17898874]
24. Mitroulis I, Kourtzelis I, Kambas K, et al. Regulation of the autophagic machinery in human neutrophils. Eur J Immunol. 2010; 40:1461–72. [PubMed: 20162553]
25. Yang CS, Lee JS, Rodgers M, et al. Autophagy protein Rubicon mediates phagocytic NADPH oxidase activation in response to microbial infection or TLR stimulation. Cell Host Microbe. 2012; 11:264–76. [PubMed: 22423966]
26. Huang J, Brumell JH. NADPH oxidases contribute to autophagy regulation. Autophagy. 2009; 5:887–9. [PubMed: 19550142]
27. Paglin S, Hollister T, Delohery T, et al. A novel response of cancer cells to radiation involves autophagy and formation of acidic vesicles. Cancer Res. 2001; 61:439–44. [PubMed: 11212227]
28. Chan LL, Shen D, Wilkinson AR, et al. A novel image-based cytometry method for autophagy detection in living cells. Autophagy. 2012; 8:1371–82. [PubMed: 22895056]
29. Johansen T, Lamark T. Selective autophagy mediated by autophagic adapter proteins. Autophagy. 2011; 7:279–96. [PubMed: 21189453]
30. Lavrentyev EN, Malik KU. High glucose-induced Nox1-derived superoxides downregulate PKC-betaII, which subsequently decreases ACE2 expression and ANG(1–7) formation in rat VSMCs. Am J Physiol Heart Circ Physiol. 2009; 296:H106–18. [PubMed: 18978194]
31. Ray PD, Huang BW, Tsuji Y. Reactive oxygen species (ROS) homeostasis and redox regulation in cellular signaling. Cell Signal. 2012; 24:981–90. [PubMed: 22286106]
32. Xiong J, Xia M, Xu M, et al. Autophagy maturation associated with CD38-mediated regulation of lysosome function in mouse glomerular podocytes. J Cell Mol Med. Nov 17.2013
33. Kochl R, Hu XW, Chan EY, et al. Microtubules facilitate autophagosome formation and fusion of autophagosomes with endosomes. Traffic. 2006; 7:129–45. [PubMed: 16420522]
34. Rubinsztein DC, Ravikumar B, Acevedo-Arozena A, et al. Dyneins, autophagy, aggregation and neurodegeneration. Autophagy. 2005; 1:177–8. [PubMed: 16874055]
35. Ravikumar B, Acevedo-Arozena A, Imarisio S, et al. Dynein mutations impair autophagic clearance of aggregate-prone proteins. Nat Genet. 2005; 37:771–6. [PubMed: 15980862]
36. Bjorkoy G, Lamark T, Pankiv S, et al. Monitoring autophagic degradation of p62/SQSTM1. Methods Enzymol. 2009; 452:181–97. [PubMed: 19200883]
37. Lin SX, Collins CA. Regulation of the intracellular distribution of cytoplasmic dynein by serum factors and calcium. J Cell Sci. 1993; 105:579–88. [PubMed: 8408287]
38. Lesich KA, Kelsch CB, Ponichter KL, et al. The calcium response of mouse sperm flagella: role of calcium ions in the regulation of dynein activity. Biol Reprod. 2012; 86:105. [PubMed: 22262695]
39. Wu GS, Zhang YW, Wang XW, et al. Effects of enamel matrix proteins loaded in chitosan thermosensitive hydrogel on bone marrow stromal cells in vitro. Shanghai Kou Qiang Yi Xue. 2009; 18:178–82. [PubMed: 19417996]
40. Xu M, Li XX, Ritter JK, et al. Contribution of NADPH oxidase to membrane CD38 internalization and activation in coronary arterial myocytes. PLoS One. 2013; 8:e71212. [PubMed: 23940720]
41. Zhang AY, Li PL. Vascular physiology of a Ca2+ mobilizing second messenger - cyclic ADP-ribose. J Cell Mol Med. 2006; 10:407–22. [PubMed: 16796808]
42. Zhang AY, Yi F, Teggatz EG, et al. Enhanced production and action of cyclic ADP-ribose during oxidative stress in small bovine coronary arterial smooth muscle. Microvasc Res. 2004; 67:159–67. [PubMed: 15020207]
43. Schmidt AM, Hori O, Brett J, et al. Cellular receptors for advanced glycation end products. Implications for induction of oxidant stress and cellular dysfunction in the pathogenesis of vascular lesions. Arterioscler Thromb. 1994; 14:1521–8. [PubMed: 7918300]
44. Twig G, Elorza A, Molina AJ, et al. Fission and selective fusion govern mitochondrial segregation and elimination by autophagy. EMBO J. 2008; 27:433–46. [PubMed: 18200046]

45. Tal MC, Sasai M, Lee HK, et al. Absence of autophagy results in reactive oxygen species-dependent amplification of RLR signaling. Proc Natl Acad Sci U S A. 106:2770–5. 200. [PubMed: 19196953]

46. Marsh BJ, Soden C, Alarcon C, et al. Regulated autophagy controls hormone content in secretory-deficient pancreatic endocrine beta-cells. Mol Endocrinol. 2007; 21:2255–69. [PubMed: 17579214]

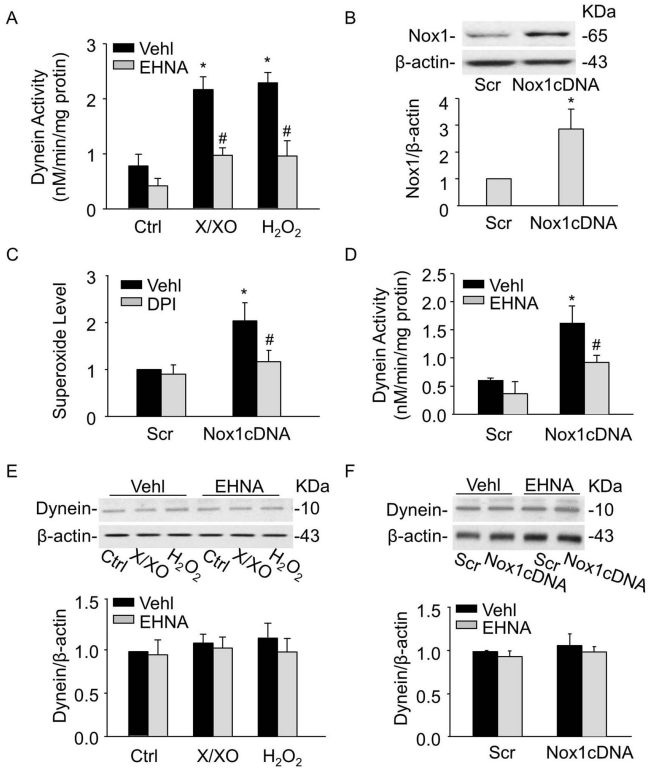

Figure 1. Regulation of dynein ATPase activity by ROS

(A) CAMs were incubated with under X/XO (10 μM/0.1 U/ml) or H_2O_2 (10 μM) for 24 hours in the presence or absence of dynein inhibitor EHNA (30 μM). Summarized data showing the dynein ATPase activity induced by X/XO or H_2O_2. (B) Representative Western blot gel document and summarized intensity ratio of Nox1 to β-actin showing the expression of Nox1 in CAMs with scramble (Scr) or Nox1 cDNA plasmids transfection. (C) Summarized ESR data showing the relative $O_2^{-\cdot}$ production in CAMs with scramble or Nox1 cDNA transfection in the absence or presence of DPI (50 μM). (D) Summarized data showing the effects of dynein inhibitor EHNA (30 μM) on dynein ATPase activity in CAMs with scramble or Nox1 cDNA transfection. (E–F) Representative Western blot gel document and summarized data showing the protein expression of dynein in CAMs under X/XO or H_2O_2 stimulation (panel E) and after Nox1 cDNA transfection (panel F). (n=6 for all panels). *P<0.05 *vs.* Ctrl or Scramble; #P<0.05 *vs.* CAMs treated with X/XO or H_2O_2 or Nox1 cDNA transfection alone.

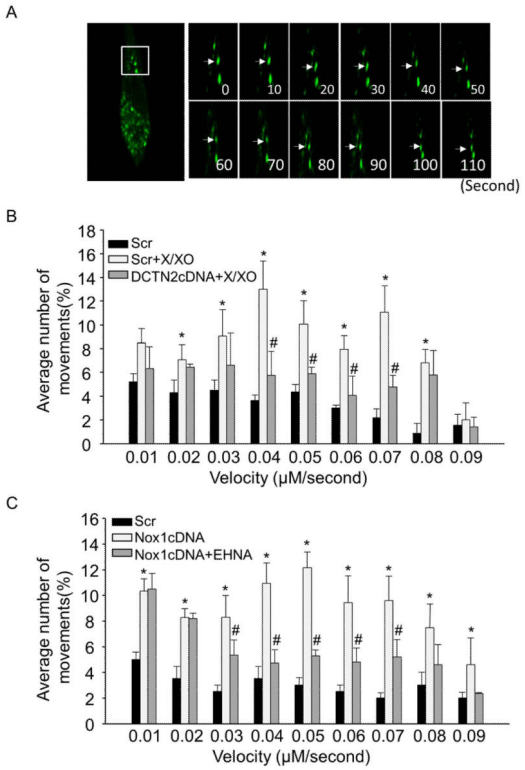

Figure 2. Analysis of AP dynamic movements

(A) Typical fluorescent images of LC3B-GFP labeled APs in CAMs were taken every 10 second in CAMs. (B, C) The summarized data show the velocity of APs in CAMs pretreated with EHNA (30 μM) or transfected with dynamitin (DCTN2) cDNA. (n=6 for all panels). **P*<0.05 *vs.* Scramble; #*P*<0.05 *vs.* CAMs with X/XO or Nox1 cDNA transfection alone.

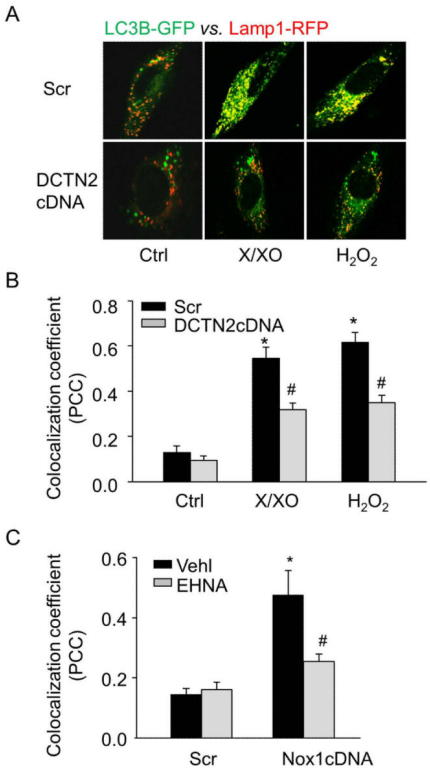

Figure 3. Inhibition of dynein activity blocked lysosome fusion

(A) Representative confocal microscopic images showing the colocalization of LC3B-GFP with Lamp1-RFP in live CAMs. (B) Summarized colocalization coefficient (PCC) of LC3B and Lamp1 in CAMs transfected with scramble or DCTN2 cDNA. (C) Summarized colocalization coefficient of LC3B-GFP and Lamp1-RFP in CAMs with or without EHNA (30 μM). (n=6 for all panels). *$P<0.05$ *vs.* Ctrl or Scramble; $^{\#}P<0.05$ *vs.* CAMs treated with X/XO or H_2O_2 or Nox1 cDNA transfection alone.

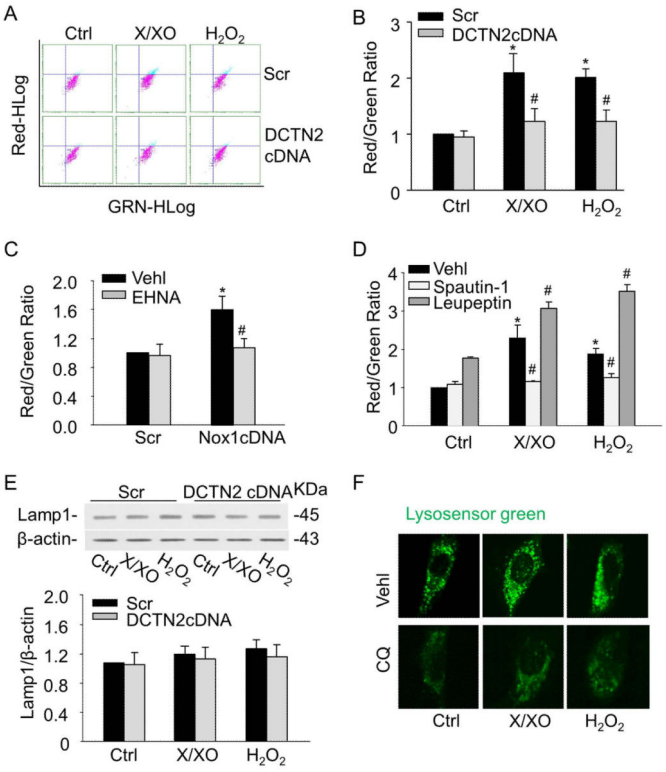

Figure 4. Inhibition of dynein activity decreased APLs formation

Mouse CAMs were stained with acridine orange for 17 minutes. Representative dot plots of flow cytometry (A) and summarized red-to-green fluorescence ratio analysis showing APLs formation in CAMs with DCTN2 cDNA (B) or EHNA (C). (D) Summarized red-to-green fluorescence ratio analysis showing APLs formation in CAMs with spautin-1 (10 μM) and leupeptin (0.25 mM). (E) Representative Western blot documents showing the expression of Lamp-1 from CAMs. (F) CAMs were treated with chloroquine (CQ, 100 μM) for 30 minutes or left untreated. They were then stained with LysoSensor Green DND-189 and analyzed by fluorescence microscopy. (n=6 for all panels). *$P<0.05$ *vs.* Scramble; $^{\#}P<0.05$ *vs.* CAMs with X/XO or H_2O_2 or Nox1 cDNA transfection alone.

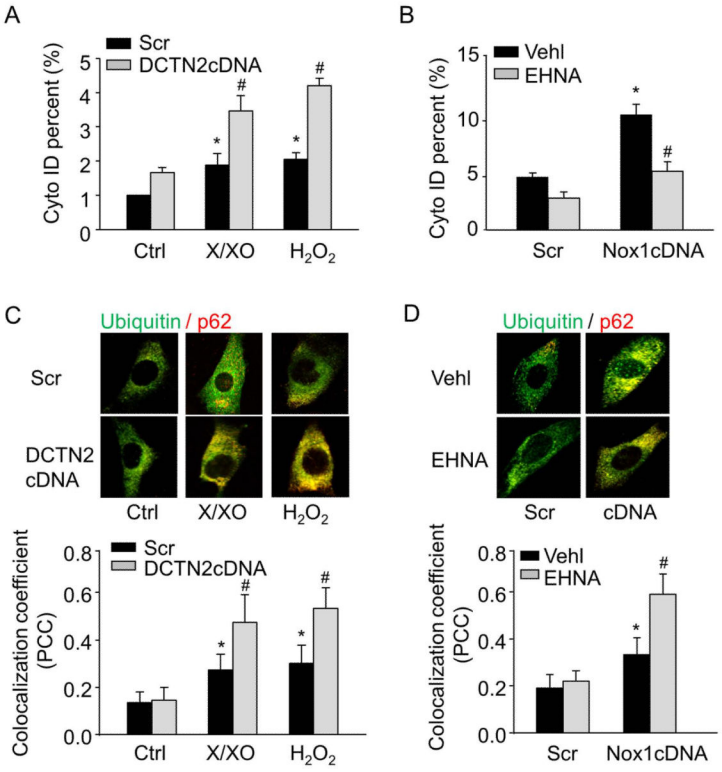

Figure 5. Dynein inhibition increased accumulation of APs and decreased breakdown of APs

(A, B) Summarized percent of Cyto-ID stained cells showing the relative number of APs in CAMs with EHNA or DCTN2 cDNA. (C, D) Representative confocal images and summarized colocalization coefficient showing the colocalization of ubiquitin with p62. (n=6 for all panels). **P*<0.05 *vs.* Ctrl or Scramble; #*P*<0.05 *vs.* CAMs treated with X/XO or H_2O_2 or Nox1 cDNA transfection alone.

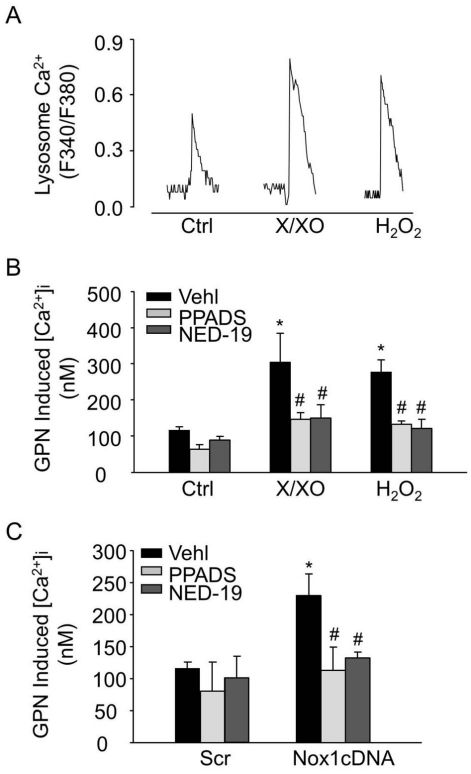

Figure 6. Lysosome Ca^{2+} release in response to ROS in living CAMs

Glycyl-l-phenylalanine-β-naphthylamide (GPN, 200 μM) was used to release Ca^{2+} from lysosomes. Representative lysosomal Ca^{2+} traces (A) and summarized data showing the effects of NAADP antagonists, PPADS (50 μM) or NED-19 (10 μM) on GPN-induced lysosomal Ca^{2+} release in CAMs treated with X/XO or H_2O_2 (B) or Nox1 cDNA (C). (n=6 for all panels). $^{*}P<0.05$ *vs.* Ctrl or Scramble; $^{\#}P<0.05$ *vs.* CAMs treated with X/XO or H_2O_2 or Nox1 cDNA transfection alone.

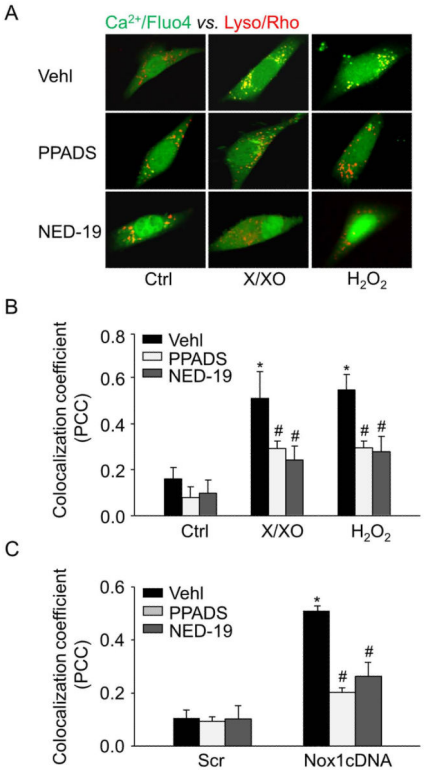

Figure 7. Confocal microscopic detection of Ca^{2+} release from lysosomes locally in CAMs

(A) Representative confocal microscopy images showing Ca^{2+} release regions that colocalized with lysosomes as shown by yellow spots formed by green fluo-4 signals with rhodamine-red lysosomal marker (Lyso/Rho). Summarized data showing the colocalization coefficienct of Ca^{2+}/fluo-4 with Lyso/Rho signals in CAMs treated with X/XO or H_2O_2 (B) or Nox1 cDNA (C). (n=6 for all panels). **P*<0.05 *vs.* Ctrl or Scramble; #*P*<0.05 *vs.* CAMs treated with X/XO or H_2O_2 or Nox1 cDNA transfection alone.

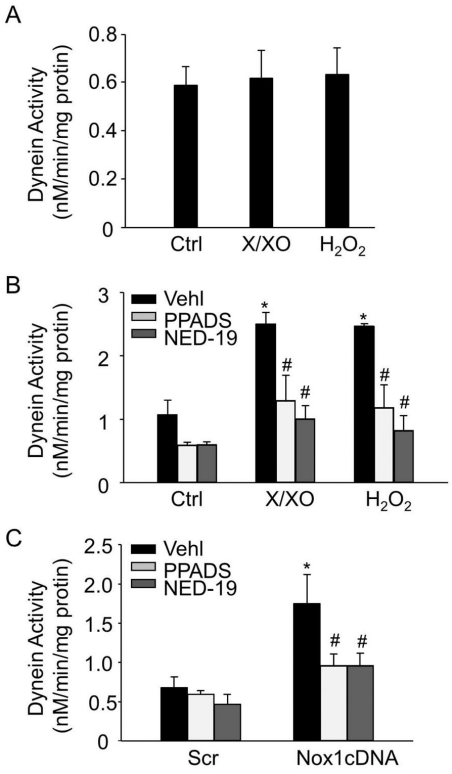

Figure 8. Lysosome Ca^{2+} signaling regulated dynein ATPase activity

(A) 10 μg proteins of isolated cytoplasmic lysates from CAMs were incubated with X/XO (10 μM/0.1 U/ml) or H_2O_2 (10 μM) for 2 hours. Summarized data showing the direct oxidizing effects of ROS on dynein ATPase activity. (B–C) Summarized data showing the effects of NAADP antagonists, PPADS (50 μM) or NED-19 (10 μM) on dynein ATPase activity in CAMs under X/XO (10 μM/0.1 U/ml) or H_2O_2 (10 μM) stimulation or Nox1 cDNA transfection in CAMs. (n=6 for all panels). $^{*}P<0.05$ *vs.* Ctrl or Scramble; $^{\#}P<0.05$ *vs.* CAMs treated with X/XO or H_2O_2 or Nox1 cDNA transfection alone.

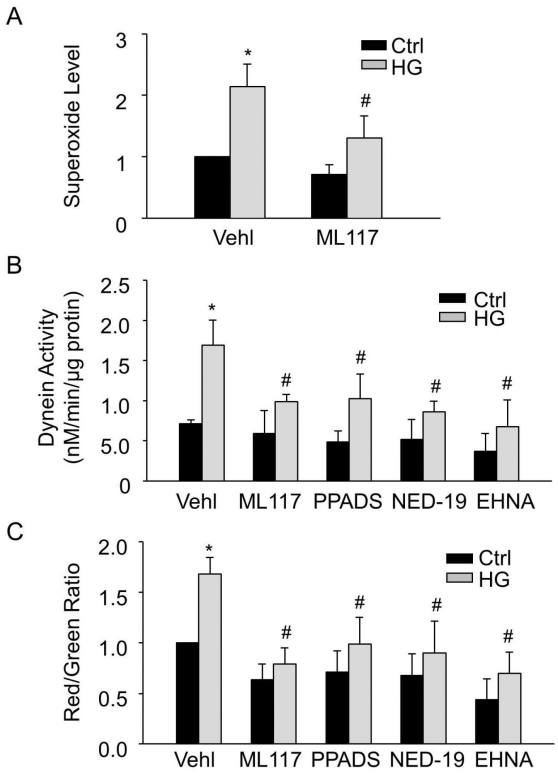

Figure 9. NAADP-lysosome Ca^{2+} controlled high glucose-induced dynein activation

(A) Summarized data showing the effects of Nox1 inhibitor ML117 (100 μM) on $O_2^{-\cdot}$ production in CAMs under control and high glucose (30 mM) for 48 hours. Summarized data showing the effects of Nox1 inhibitor ML117, dynein inhibitor EHNA and NAADP antagonists PPADS or NED-19 on dynein ATPase activity (B) or APLs formation (red-to-green fluorescence ratio of acridine orange) (C) in CAMs under resting control condition or with high glucose. (n=6 for all panels). **P*<0.05 *vs.* Ctrl; $^{\#}P$<0.05 *vs.* CAMs treated with high glucose.